Interface Polar Symmetry Induced Piezoelectric and Pyroelectric Effects

Ming-Min Yang[1,4]*, Zheng-Dong Luo[1], Zhou Mi[2], Jinjin Zhao[2], Sharel Pei E[3], Marin Alexe[1]*

[1]Department of Physics, the University of Warwick, Coventry, CV4 7AL, United Kingdom.

[2]School of Materials Science and Engineering, School of Mechanical Engineering, Shijiazhuang Tiedao University, Shijiazhuang, 050043, China.

[3]Warwick Manufacturing Group, the University of Warwick, Coventry, CV4 7AL, United Kingdom.

[4]Present address: Center for Emergent Matter Science, RIKEN, Wako, Saitama, 351-0198, Japan.

* E-mail: ymmwhut@gmail.com; m.alexe@warwick.ac.uk

Interfaces in heterostructures have been a key focal of interest in condensed matter physics for decades owing to a plethora of distinctive phenomena and their critical roles in nowadays technical devices, such as rectification[1], photovoltaic effect[2], quantum Hall effect[3] and high temperature superconductivity[4], etc. However, the symmetry modulation at interfaces and the resultant effects have been largely overlooked. Here we show that a band bending (i.e. electric field) at interfaces induces polar symmetry therein and gives rise to emergent functionalities, including piezoelectricity and pyroelectricity, even though the component materials are centrosymmetric. We study here a classic interface, namely Schottky junction, formed by noble metal and centrosymmetric semiconductors including Nb-doped Nb:$SrTiO_3$, Nb:TiO_2 crystals, Nb:$Ba_{0.6}Sr_{0.4}TiO_3$ ceramics and silicon. The built-in electric field in the depletion region induces polar structures in semiconductors and generates substantial piezoelectric and pyroelectric effects. In particular, the interface pyroelectric coefficient and figure of merit are over one order magnitude larger than conventional bulk polar materials. Our study enriches the functionalities of heterostructure interfaces, offering a distinctive approach to realize energy transduction beyond the conventional limitation imposed by intrinsic symmetry.

The symmetry lies at the heart of the nature laws and forms the basis for the modern physics that determines material properties at the fundamental level.[5] Breaking the inversion symmetry allows emergent functionalities and effects. For example, the piezoelectric effect, that converts mechanical energy into electricity and vice versa in a linear manner, is restricted to non-centrosymmetric materials.[6] The pyroelectric effect, which transforms thermal energy into electric energy, only occurs in materials with polar symmetry.[7] Material symmetry is generally determined by its pristine crystallographic structure and loss of symmetry usually happens via phase transitions. For instance, the paraelectric-to-ferroelectric phase transition in $BaTiO_3$ reduces the crystals symmetry from centrosymmetric cubic to polar tetragonal, making $BaTiO_3$ piezoelectric and pyroelectric.[6,7]

Nevertheless, the material symmetry can also be tuned by external stimuli that lower the symmetry, or even break the inversion symmetry, of any centrosymmetric material.[8,9] One of the prominent examples is the strain gradient which parameterizes the inhomogeneity of the strain developed in materials. Strain gradients break the inversion symmetry and induce an electric polarization in materials of any symmetry by so-called flexoelectric effect.[10] This symmetry breaking is associated with a variety of emergent functionalities such as piezoelectric, pyroelectric and bulk photovoltaic effects for any materials such as centrosymmetric $SrTiO_3$ and TiO_2.[11-15] Despite its universal nature, the real application of this intriguing flexoelectric effect is hampered by its rather small effective coefficients and a complicated setup for inducing large strain gradients. Thus, an alternative would be highly desirable for developing or tuning applications based on induced symmetry breaking.

In this regard, electric field can play the similar role as the strain gradient in terms of symmetry engineering.[8,16] It has already been employed in two-dimensional systems to engineer their non-centrosymmetry to introduce functionalities with applications in spintronics[17], valleytronics[18], photogalvanic effect[19], etc. The electric field can induce in principle a more general symmetry breaking and not only those mentioned above. As claimed by Nye[8], a crystal under an external stimulus will only exhibit those symmetry elements that are common to both the pristine crystal and the stimulus (Fig. 1a). For example, applying an electric field, which is a vector possessing the conical symmetry of ∞m, to a cubic $SrTiO_3$ crystal with a point symmetry group of $m\bar{3}m$, leads to the common point group of 4mm that is polar. Accordingly, the $SrTiO_3$ crystal subjected to the electric field along its (001) direction will not any more exhibit its original cubic symmetry but the polar symmetry (see Methods and Extended Data Fig. 1). Therefore, the electric field not only breaks the inversion symmetry but also induces polar structures in centrosymmetric materials. The electric field can be both externally applied and built-in fields, the latter usually originating from band bending or chemical potential gradient that are generally found at heterostructure interfaces. In this study, we show that an electric field manifesting at interfaces can induce polar symmetry and give rise to emergent piezoelectric and pyroelectric effects in centrosymmetric materials, that are otherwise forbidden. We also show here that these interface effects can be not only artificially induced in any heterostructures, but also rationally tuned to a magnitude much larger than that of conventional bulk materials.

The model systems that usually show a rather strong built-in filed are metal-semiconductor contacts termed Schottky junctions. Rearrangement of the energy levels in order to align the Fermi level in both metal and semiconductor generates band bending and a depletion region within the

semiconductor associated with an electric field pointing from the semiconductor to the noble metal (Fig. 1b).[1] Accordingly, polar structures are induced in the depletion region of the centrosymmetric semiconductors. The coefficient of the induced piezoelectric effect associated with a Schottky junction can be predicted as (see Methods):

$$d_{ijk} = Q_{jki3}\chi_3\sqrt{2qN_d\chi_3 V_{bi}} \quad (1)$$

where Q_{jki3} is the electrostriction coefficient, χ_3 is the dielectric permittivity in the field direction, q is the elemental charge, N_d is the effective donor density, V_{bi} is the built-in potential in the Schottky junction. For the sake of simplicity, the most basic Schottky model is used here to describe the potential profile at the metal/semiconductor interface without considering, for example, interface insulating layer and interface states.[20] Clearly, the piezoelectric coefficient is determined by the centrosymmetric semiconductor properties, such as the dielectric permittivity and the dopant density. A phenomenological theory has also been established to unravel the microscopic mechanism of the interface piezoelectric effect (see Methods and Extended Data Fig. 2). Both direct and converse interface piezoelectric effects arise from the combination of the built-in field and the electrostriction effect.

To quantitatively evaluate the piezoelectric coefficient, high-quality Schottky junctions have been fabricated by sputtering noble metal (i.e. gold) on (001)-oriented Nb-doped $SrTiO_3$ (Nb:STO) and Nb-doped TiO_2 (Nb:TO) single crystals (Methods). For the Au/Nb:STO junction, generic electrical properties have been determined by performing current-voltage and capacitance-voltage measurements (Fig. 1c,d). Note that aluminium evaporated on the same surface of the Nb:STO crystal forms ohmic contacts, which are used as the counter electrodes with the Schottky junctions (Extended Data Fig. 3). The Au/Nb:STO junction exhibits an excellent rectification effect with a current density ratio reaching about 10^9 at ±1.5 V and a large capacitance at zero external bias (C=4.7 μF/cm^2). The dependence of reciprocal value of squared capacitance on external bias is given by:[1]

$$C(V)^{-2} = \frac{2V_{bi}}{q\chi_3 N_d} - \frac{2V}{q\chi_3 N_d} \quad (2)$$

By performing linear fitting of $C(V)^{-2}$ vs V, we obtain the values for following parameters: $\chi_3 = 1.68 \times 10^{-9}$ C/Vm (ε_r= 190) and V_{bi}=1.43 V (inset of Fig. 1d). From the Hall effect we obtain the doping density N_d=2.4×10^{25} m^{-3}. Given the Nb:STO electrostriction coefficient Q_{11}=0.046 m^4/C^2 and Q_{12}=-0.013 m^4/C^2 (ref. 21), the corresponding piezoelectric coefficients are estimated from Eq.

1 to be d_{33}=10 pm/V and d_{31}=-3 pm/V. These coefficients are in the same order of magnitude of widely used piezoelectric materials such as $LiNbO_3$ (d_{31}=-2.59 pm/V).[22]

To experimentally verify the existence and quantitatively evaluate the magnitude of the interface piezoelectric effect in Schottky junctions, we measured the direct piezoelectric effect by applying a dynamic stress to the parallel crystal edges and measuring the short-circuit current generated by the junction (Fig. 2a and Methods). Particular care has been taken in order to apply the stress homogeneously, minimising any contributions from the inhomogeneous strain and thus flexoelectric effect.[10] As shown in Fig. 2b, under the stimulus of a sinusoidal stress with an amplitude of σ_1=7.9 MPa and a frequency of f=500 Hz, the Au/Nb:STO junction outputs an alternative current with the same frequency and an amplitude of J=10.1 μA/cm^2. More importantly, the amplitude of output current density increases linearly with the amplitude of the applied stress, demonstrating the manifestation of the direct piezoelectric effect in the Au/Nb:STO junction (Fig. 2c). The corresponding piezoelectric coefficient calculated as $d_{31} = \frac{J}{2\pi f \sigma_1} = -4.07$ pC/N is close to the value predicted above. To demonstrate that the interface piezoelectricity is a universal effect rather than a phenomenon just limited to the Nb:STO crystals, we performed the same measurements on another centrosymmetric semiconductor, i.e. Nb:TiO_2 and its Schottky junction with gold. Estimation assuming the same electrostriction coefficient as the $SrTiO_3$ crystal predicts a piezoelectric constant with a magnitude of 1.52 pC/N for Au/Nb:TO junctions (Extended Data Fig. 3). The measured piezoelectric coefficient of the Au/Nb:TO junctions is about 0.97 pC/N, which is close with our prediction (Fig. 2c). Note that the Nb:STO and Nb:TO crystals with Ohmic contacts do not show any piezoelectric effect and generate no electricity under the mechanical stimuli, confirming the critical role of the Schottky junctions in generating the piezoelectric effect (Extended Data Fig. 4).

For further confirmation, we explored the converse piezoelectric effect in the Schottky junction by applying an alternative bias to the junction and measuring the resulting surface displacement via atomic force microscope (see Methods). The surface displacement of the Au/Nb:STO junction increases linearly with the amplitude of the excitation voltage, leading to a piezoelectric coefficient of d_{33}=16.3 pm/V, which is similar to the value estimated above (Fig. 2d). These results clearly demonstrate that the heterostructures of centrosymmetric materials with an interface built-in field possess both direct and converse piezoelectric effect just like the conventional bulk non-centrosymmetric materials.

As mentioned previously, the built-in field within the Schottky junction not merely lifts-off the inversion symmetry, but also induces local polarisation via the polar nature of the field. Thus, in addition to the piezoelectric effect, the Schottky junction shall also show pyroelectric effect that is the finger-print feature of any polar structures.[7] This interface pyroelectric effect originates from the temperature dependence of the dielectric permittivity, effective dopant density and built-in potential in Schottky junctions (see Eq.18 in Methods). To demonstrate this scenario, we measured the pyroelectric effect in Schottky junctions by dynamically modulating their temperature and measuring the generated short-circuit current (Methods). When its temperature is being sinusoidally modulated, the Au/Nb:STO junction outputs an alternating current with a phase shift of 90^{o}, confirming the manifestation of the pyroelectric effect at Schottky junctions (Fig. 3a). The corresponding pyroelectric coefficient of the Au/Nb:STO junction reaches 298 $\mu C/m^2K$ at room temperature. The Au/Nb:TO junction also exhibits the pyroelectric effect with a room temperature coefficient of 312 $\mu C/m^2K$ (Fig. 3b). Both values are comparable to that of the classical pyroelectric materials.[7]

Having demonstrated the interface polar symmetry induced piezoelectricity and pyroelectricity in the Schottky junctions, we further explore their potential by enhancing their coefficients. As indicated by Eq. 1 and discussed in the Methods, the magnitude of both interface piezoelectric and pyroelectric effects depends on the doping density, dielectric permittivity and their tuneability with respect to stress, electric field and temperature. Thus, Schottky junctions consisting of semiconductors with a large dielectric tuneability are expected to exhibit both enhanced piezoelectric and pyroelectric effects. To this end, we chose 0.1%wt Nb-doped $Ba_{0.6}Sr_{0.4}TiO_3$ (Nb:BSTO) ceramics to form Schottky junctions with gold. It is known that undoped $Ba_{0.6}Sr_{0.4}TiO_3$ ceramics show a paraelectric to ferroelectric transition around -2 ^{o}C, giving rise to a substantial dielectric tuneability with a dielectric constant of ε_r= 5300 at room temperature.[23] Nevertheless, both $Ba_{0.6}Sr_{0.4}TiO_3$ and Nb:BSTO are centrosymmetric at room temperature, being in their cubic phase. The general electrical characterization of the Au/Nb:BSTO junction is given in Extended Data Fig. 5 and the preparation details are given in the Methods. As demonstrated in Fig. 2c, this junction exhibits a substantial piezoelectric effect with a coefficient d_{31}=-12 pC/N, which is about three orders of magnitude higher than that of the undoped $Ba_{0.6}Sr_{0.4}TiO_3$ ceramics.[24] In contrast, Nb:BSTO ceramic with quasi-ohimc contact exhibit negligible piezoelectric effect (Extended Data Fig. 6). More striking, the Au/Nb:BSTO junction shows a large pyroelectric effect with room temperature coefficient reaching 5.3 mC/m^2K (Fig 3b). The obtained pyroelectric coefficient here is

over one order of magnitude larger than conventional ferroelectric materials, such as $LiTaO_3$ crystal (230 μC/m^{2}K) widely used in the fabrication of pyroelectric detectors.[7] In addition to their large coefficients, the interface pyroelectric effect in Schottky junctions exhibits another two distinctive features in comparison to conventional bulk materials. Firstly, the pyroelectric effect in conventional ferroelectric materials possesses a strong temperature dependence, i.e., pyroelectric coefficients decay sharply away from the phase transition temperature, inevitably limiting their working temperature of practical devices. In contrast, the pyroelectric coefficient in the Au/Nb:BSTO junction exhibits a weak temperature dependence cross the phase transition region and remains large magnitudes over a wide temperature range, due to the persistence of the depletion region (Fig. 3b). Similarly, the pyroelectric coefficients in both Au/Nb:STO and Au/Nb:TO junctions increase monotonically with temperature, supporting their wide working temperature range. Secondly, the interface pyroelectric effect has a rapid response to the thermal perturbation. Fig.3c,d show the time dependence of the pyroelectric current generated by the Au/Nb:BSTO junction and a commercial $Pb(Ti_{0.8}Zr_{0.2})O_3$ ceramics under the same red light pulsed illumination. Clearly, the pyroelectric response of Au/Nb:BSTO ceramic is over one order of magnitude larger than that of the poled $Pb(Ti_{0.8}Zr_{0.2})O_3$ ceramic. Moreover, the thermal time constant is three orders of magnitude shorter (about 300 μs) than that of the bulk $Pb(Ti_{0.8}Zr_{0.2})O_3$ ceramic (300 ms) of similar dimensions.

We emphasis two main features of these effects arising from the interface polar symmetry. First, both piezoelectric and pyroelectric coefficients observed in the metal/semiconductor interfaces surpass that of the conventional polar materials. Although the interface piezoelectric constants are smaller than these of ferroelectric materials with switchable polarizations (e.g. $BaTiO_3$ crystals), they still rival that of non-switchable polar materials, such as ZnO and CdS etc (Fig. 4a). For example, the piezoelectric constant of the Au/Nb:BSTO junction is over twice larger than that of the ZnO crystals along with a similar electromechanical coupling factor (Methods).[25] Apart from oxide semiconductors, there is still large space to enhance the interface piezoelectric coefficient by exploring a wide range of semiconductors with large electrostriction effect, such as the organic-inorganic halide perovskites wherein the electrostriction coefficient is over three order of magnitude larger than that of $SrTiO_3$ crystal.[26] Remarkably, the interface pyroelectric effect is significantly larger than that of conventional polar materials, even the best ferroelectrics. The Schottky junctions exhibits both substantial pyroelectric coefficient and large figure of merit $F_V = p_i/c_p\chi_3$ where c_p is the heat capacity (see Fig.4b and Methods). Especially, the Au/Nb:BSTO interface shows a figure of merit of 2.11 m^2/C that is one order of magnitude larger than classic ferroelectric materials, such

as $LiTaO_3$ crystal (F_V=0.17 m^2/C).[7] This enhanced figure of merit in the Schottky junction originates from the large pyroelectric coefficient and built-in field depressed dielectric permittivity in the depletion region.

Interface piezoelectric and pyroelectric effects are universal effects applicable to materials of any symmetry. These effects arise at the heterostructures wherever an electric field builds at the interface. It is worth noting that the electric field is ubiquitous at interfaces of dissimilar materials due to the chemical potential inhomogeneity across interfaces. To validate this scenario, we studied the piezoelectric and pyroelectric effects of Schottky junctions on silicon wafer. The Au/Si (001) junction outputs a dynamic electrical current of which amplitude increases linearly with that of the applied stress (Fig. 4c). This corresponds to a low but finite piezoelectric constant of about -0.013 pC/N. Moreover, the silicon Schottky junction exhibits a sizable pyroelectric effect with a room temperature coefficient of 200 $\mu C/m^2K$ and a figure of merit of F_V=1.17 m^2/C (Fig. 4b).

In summary, we demonstrated the interface piezoelectric and pyroelectric effects which not only exhibits substantial coefficients but also is free from the symmetry limitation. They can be found and are applicable to a wide range of materials starting from conventional semiconductors, oxides, to halide perovskites and two-dimensional materials. These features open the door for their practical applications in the realm of electromechanical and thermal effects, such as energy conversion, infrared sensors, etc., with distinctive mechanisms and additional tuning feasibility different from that of intrinsic non-centrosymmetric materials. With careful designs, the interface polar effects can also work concurrently with bulk effects arising from inherent[7,8] or externally induced polarity by, e.g. strain gradients[10-15], to achieve an enhanced piezo-/pyroelectric coefficients or even new effects.

References

1 Sze, S. M. & Ng, K. K. *Physics of semiconductor devices*. (John wiley & sons, Hoboken, 2006).

2 Fahrenbruch, A. & Bube, R. *Fundamentals of solar cells: photovoltaic solar energy conversion*. (Academic Press, New York, 1983).

3 Klitzing, K. v., Dorda, G. & Pepper, M. New method for high-accuracy determination of the fine-structure constant based on quantized Hall resistance. *Phys. Rev. Lett.* **45**, 494-497 (1980).

4 Gozar, A. *et al.* High-temperature interface superconductivity between metallic and insulating copper oxides. *Nature* **455**, 782-785 (2008).

5 Livio, M. Why symmetry matters.*Nature* **490**, 472-473 (2012)

6 Mason, W. P. & Baerwald, H. *Piezoelectric crystals and their applications to ultrasonics*. (D. Van Nostrand Company, Inc, New York, 1950).

7 Whatmore, R. Pyroelectric devices and materials. *Rep.Prog.Phys.* **49**, 1335-1386 (1986).

8 Nye, J. F. *Physical properties of crystals: their representation by tensors and matrices*. (Oxford university press, Oxford, 1985).

9 Bir, G. L. & Pikus, G. E. *Symmetry and strain-induced effects in semiconductors*. (John Wiley & Sons, New York, 1974).

10 Zubko, P., Catalan, G. & Tagantsev, A. K. Flexoelectric effect in solids. *Annu. Rev. Mater. Res.* **43**, 387-421 (2013).

11 Zubko, P., Catalan, G., Buckley, A., Welche, P. R. & Scott, J. F. Strain-gradient-induced polarization in $SrTiO_3$ single crystals. *Phys. Rev. Lett.* **99**, 167601, (2007).

12 Narvaez, J., Vasquez-Sancho, F. & Catalan, G., Enhanced flexoelectric-like response in oxide semiconductors, *Nature* **538**, 219-221 (2016).

13 Yang, M.-M., Kim, D. J. & Alexe, M. Flexo-photovoltaic effect. *Science* **360**, 904-907 (2018).

14 Yang, M. M., Iqbal, A. N., Peters, J. J. P., Sanchez, A. M. & Alexe, M. Strain-gradient mediated local conduction in strained bismuth ferrite films. *Nat. Commun.* **10**, 2791 (2019).

15 Meirzadeh, E. *et al.* Surface Pyroelectricity in Cubic $SrTiO_3$. *Adv. Mater.* **31**, 1904733, (2019).

16 Cheong, S.-W. SOS: symmetry-operational similarity. *npj Quant. Mater.* **4**, 53 (2019).

17 Papadakis, S., De Poortere, E., Manoharan, H., Shayegan, M. & Winkler, R. J. S. The effect of spin splitting on the metallic behavior of a two-dimensional system. *Science* **283**, 2056-2058 (1999).

18 Wu, S. *et al.* Electrical tuning of valley magnetic moment through symmetry control in bilayer MoS_2. *Nat. Phys.* **9**, 149-153 (2013).

19 Yuan, H. *et al.* Generation and electric control of spin-valley-coupled circular photogalvanic current in WSe_2. *Nat. Nanotechnol.* **9**, 851-857 (2014).

20 Suzuki, S. *et al.* Fabrication and characterization of $Ba_{1-x}K_xBiO_3$/Nb-doped $SrTiO_3$ all-oxide-type Schottky junctions. *J. Appl. Phys.* **81**, 6830-6836 (1997).

21 Alexander K. and Tagantsev, A.K. Positive effective Q_{12} electrostrictive coefficient in perovskites, *J. Appl. Phys.* **112**, 094106 (2012);

22 Yamada, T., Niizeki, N., Toyoda, H. Piezoelectric and elastic properties of lithium niobate single crystals, *Jpn. J. Appl. Phys.* **6** 151-155 (1967).

23 Samara, G. A. Pressure and temperature dependences of the dielectric properties of the perovskites $BaTiO_3$ and $SrTiO_3$. *Phys. Rev.* **151**, 378-386 (1966).

24 Biancoli, A., Fancher, C. M., Jones, J. L. & Damjanovic, D. Breaking of macroscopic centric symmetry in paraelectric phases of ferroelectric materials and implications for flexoelectricity. *Nat. Mater.* **14**, 224-229 (2015).

25 Kobiakov, I. B. Elastic, piezoelectric and dielectric properties of ZnO and CdS single crystals in a wide range of temperatures. *Solid State Commun.* **35**, 305-310 (1980).

26 Chen, B. et al. Large electrostrictive response in lead halide perovskites. *Nat. Mater.* **17**, 1020-1026 (2018).

27 Mangalam, R. V. K., Agar, J. C., Damodaran, A. R., Karthik, J. and Martin, L. W. Improved pyroelectric figures of merit in compositionally graded $PbZr_{1-x}Ti_xO_3$ thin films, *ACS Appl. Mater. Interfaces* **5**, 13235-13241 (2013).

Main Figure Legends

Fig. 1| Crystal symmetry engineering and Schottky junction electrical characterization. a, Schematic illustration of the principle of crystal symmetry engineering by external stimulus. **b**, Schematic of a Schottky junction showing the potential variation in the depletion region, where E_F is the Fermi level, Φ_B is the barrier height, V_{bi} is the built-in potential, W is the depletion region and E denotes the field. **c**, Current-voltage curve and **d**, Capacitance-voltage curve of the Au/Nb:$SrTiO_3$/Al junction. Inset of (d) shows the C^{-2} as a function of applied voltage and its linear fit.

Fig. 2| Interface piezoelectric effect. a, Schematic illustrating the device used to characterize the direct piezoelectric effect of Schottky junctions. **b**, Waveform of the current density generated by the Au/Nb:$SrTiO_3$/Al junction under the stimulus of a sinusoidally varied stress. **c**, Stress dependent current density generated in Au/Nb:$SrTiO_3$/Al, Au/Nb:TiO_2/Al and Au/Nb:$Bb_{0.6}Sr_{0.4}TiO_3$/Al junctions, respectively. The solid lines are their linear fits. **d**, Surface displacement of the Au/Nb:$SrTiO_3$ junction as a function of the amplitude of applied AC voltage. The line is the linear fit.

Fig. 3| Interface pyroelectric effect. a, Waveform of the temperature variation in the Au/Nb: $SrTiO_3$ junction along with the waveform of the generated pyroelectric current density. **b**, Temperature dependence of pyroelectric coefficients of the Au/Nb:$SrTiO_3$, Au/Nb:TiO_2 and Au/Nb:BSTO Schottky junctions. Pulsed light induced transient pyroelectric current in **c**, Au/Nb:BSTO junction and **d**, $Pb(Ti_{0.8}Zr_{0.2})O_3$ ceramic, respectively.

Fig. 4| Giant magnitude and universal nature of the interface polar effects. **a**, Interface piezoelectric constant d_{31} and its electromechanical coupling factors k_{31} in comparison with conventional polar materials. **b**, Comparation of the pyroelectric coefficients and figure of merit of the studied devices with that of ferroelectric materials. **c**, The amplitude of current density generated in Au/Si junctions as a function of the amplitude of applied stress. Piezoelectric and pyroelectric data on bulk materials are taken from ref. 7, 22, 25, 27.

Methods

Symmetry analysis of (001)-oriented Nb:$SrTiO_3$ and Nb:TiO_2 Schottky junctions: The Nb:$SrTiO_3$ single crystal belongs to the point symmetry group of $m\bar{3}m$ that includes the symmetry elements of (1, $2_{\{100\}}$, $2_{\{110\}}$, 3, 4, $\bar{1}$, $\bar{3}$, $\bar{4}$, $m_{\{100\}}$, $m_{\{110\}}$). The electrical field in the Schottky junction of Nb:$SrTiO_3$ crystal points along the (001) direction. Due to its vector nature, the field exhibits the symmetry of ∞m that includes two types of symmetry elements, i.e. infinite rotation symmetry along (001) direction and infinite mirror symmetry. The ∞m symmetry can be represented by a cone. Due to the manifestation of the electrical field in the Schottky junction, the depletion region will only exhibit the point symmetry which is the subgroup to both m$\bar{3}$m and ∞m. As illustrated in Extended Data Fig.1a, the symmetry elements common to both symmetry groups are (1, $2_{(001)}$, $4_{(001)}$, $m_{(100)}$, $m_{(010)}$, $m_{(110)}$, $m_{(1\text{-}10)}$). The resultant group of symmetry elements corresponds to the point group of 4mm which represents polar structures, such as that of $BaTiO_3$ in the tetragonal phase. Similarly, the rutile Nb:TiO_2 possesses the point group of 4/mmm which includes symmetry elements of (1, $2_{\{100\}}$, $2_{(1\text{-}10)}$, $2_{(110)}$, $4_{(001)}$, $\bar{1}$, $\bar{4}$, $m_{\{100\}}$, $m_{(1\text{-}10)}$, $m_{(110)}$). Its common sub-group with ∞m is also the point group $4mm$ (Extended Data Fig.1b).

Interface piezoelectricity at Schottky junction. If the work function of the metal exceeds that of the semiconductor, a Schottky barrier forms at the interface between metal and semiconductor (Fig. 1b). In the ideal case, the depletion width W is given by[1]:

$$W = \sqrt{\frac{2\chi_3}{qN_d}(V_{bi} - V - \frac{kT}{q})} \quad (3)$$

where χ_3 is the dielectric permittivity, q is the electron charge, N_d is the density of dopant, V_{bi} is the built-in voltage, V is the external applied bias, k is the Boltzmann constant, T is the absolute temperature. Since the term kT/q is usually much smaller than V_{bi} in the case of interest, Eq. 3 can be simplified as:

$$W = \sqrt{\frac{2\chi_3}{qN_d}(V_{bi} - V)} \quad (4)$$

The potential variation in the depletion region is given as:

$$V(x) = \frac{qN_d}{\chi_3}\left(Wx - \frac{1}{2}x^2\right) - \Phi_B \quad (5)$$

where Φ_B is the barrier height at metal-semiconductor interface. Thus, the corresponding field is:

$$E(x) = \frac{\partial V}{\partial x} = \frac{qN_d}{\chi_3}(W - x) \quad (6)$$

Therefore, the local strain in the depletion region induced by the electrostriction effect can be predicted as:

$$\varepsilon(x) = ME^2 = M\left(\frac{qN_d}{\chi_3}\right)^2 (W - x)^2 \quad (7)$$

where M is the electrostriction coefficient (in its one-dimensional form) in the unit of m^2/V^2. The total displacement over the depletion region then:

$$\Delta L = \int_0^W \varepsilon(x)dx = \frac{1}{3}M\left(\frac{qN_d}{\chi_3}\right)^2 W^3 = \frac{2}{3}M\sqrt{\frac{2qN_d}{\chi_3}}(V_{bi} - V)^{\frac{3}{2}} \quad (8)$$

If an AC voltage with following form:

$$V = V_a sin\omega t + V_0 \quad (9)$$

is applied on the junction, the corresponding displacement would be given by:

$$\Delta L = \frac{2}{3}M\sqrt{\frac{2qN_d}{\chi_3}}(V_{bi} - V_a sin\omega t - V_0)^{\frac{3}{2}} \quad (10)$$

Due to the nonlinear exponent, the Schottky junction would generate a first-order harmonic displacement (i.e. strain), which can be obtained by calculating the Fourier series of above equation. In the first approximation the displacement is given by:

$$\Delta L_{f_0} = MV_a \sin\omega t \sqrt{\frac{2qN_d}{\chi_3}(V_{bi} - V_0)} \quad (11)$$

Therefore, the Schottky junction behaves similar to a classical piezoelectric material whose strain varies linearly with applied bias. The effective piezoelectric constant d_{eff} is

$$d_{eff} = \frac{\Delta L_{f_0}}{V_a} = M\sqrt{\frac{2qN_d}{\chi_3}(V_{bi} - V_0)} \quad (12)$$

By substituting the electrostriction coefficient from M (m^2/V^2) with a more fundamental parameter Q ($M = Q\chi_s^2$) with the unit of m^4/C^2:

$$d_{eff} = Q\chi_3\sqrt{2qN_d\chi_3(V_{bi} - V_0)} \quad (13)$$

According the developed phenomenological theory (see below), the Schottky junction would possess simultaneously the direct and converse piezoelectricity with the same coefficient. Thus, the piezoelectric coefficient of the Schottky junction can be given in the tensor form:

$$d_{ijk} = Q_{jki3}\chi_3\sqrt{2qN_d\chi_3(V_{bi} - V_0)} \quad (14)$$

In the case without any external bias, the Schottky junction exhibits piezoelectric tensor as:

$$d_{ijk} = Q_{jki3}\chi_3\sqrt{2qN_d\chi_3 V_{bi}} \quad (15)$$

The depletion region in the Schottky junction behaves like an insulating polar thin layer with electric polarization pointing from the semiconductor bulk to the noble metal interface, as indicated by the red arrow in the Extended Data Fig.2a. In the equilibrium state, this positive end of electric dipole is compensated by the electrons in the metal interface while the negative charge of the dipole is compensated by the positive charge in depletion region of the semiconductor. As demonstrated in the phenomenology theory, the interface piezoelectric effect originates from the combination of the built-in field and the electrostriction effect. Note that, the electrostriction effect not only describes the electric field-induced strain with a quadratic dependence but also is a measure of the dependence of the dielectric permittivity on external stress.

Once the junction is subjected to an external stress, e.g. a tensile stress perpendicular to the junction interface, the dielectric permittivity of the semiconductor will increase due to the positive electrostriction coefficient Q_{11}. This increased permittivity will give rise to an enhanced electric polarization in the depletion region, which breaks the screening equilibrium at the interface. Therefore, the increased polarization will redistribute the charge between metal and semiconductors to reach a new equilibrium state. Since the Schottky barrier prevents the electrons from directly flowing cross the interface, the electron will flow through the external circuit, giving rise to a displacive electric current (Extended Data Fig.2b). Similarly, when the junction is subjected to an external electric field, the built-in potential and field will be changed, which will modulate the strain state of the depletion region via the electrostriction effect. This electric field modulated strain leads to the converse piezoelectric effect.

Overall, the microscopic processes of the interface effects rely on the tunability of semiconductor parameters, especially the dielectric permittivity, with respect to external stimuli. As a fundamental parameter, the dielectric permittivity influences almost all the properties of Schottky junctions, such as the capacitance, depletion width, built-in field and voltage, etc. Therefore, the modulation of electric polarization by external stimuli, which is intrinsically associated with the interface piezo/pyroelectric effect, is accompanied by the variation of all the other junction properties. They are entangled to the piezo/pyroelectric effects.

It is worth noting that the interface piezoelectric effect demonstrated here is distinctive from the surface piezoelectricity, the mechanism and coefficients of which remain elusive.[28] It is also different from the flexoelectric effect in semiconductive oxides, the physics of which was constructed based on the surface piezoelectricity, one of the contributions to the flexoelectricity.[12,28] The flexoelectric effect only works with strain gradient, i.e. inhomogeneous strain. In contrast, the interface piezoelectric effect is due to the electric field induced polar symmetry and electrostriction effect, which works in any strain state, including non-strained or homogenous and inhomogeneous strained systems.

Preliminary theory of interface pyroelectric effect: The space charge Q_{SC} per unit area in the Schottky junction is given as:[1]

$$Q_{SC} = \sqrt{2q\chi_3 N_d \left(V_{bi} - V - \frac{kT}{q}\right)} \tag{16}$$

In the case without applying external bias, Eq. 16 can be rewritten as

$$Q_{SC} = \sqrt{2q\chi_3 N_d V_{bi}} \tag{17}$$

This unit area space charge Q_{SC} can be regarded as the effective polarization of the Schottky junction, which is a function of dielectric permittivity χ_3, dopant density N_d and built-in potential V_{bi}. Therefore, the pyroelectric coefficient of the Schottky junction is

$$\begin{aligned} p_i = \frac{dQ_{SC}(\chi_3, N_d, V_{bi})}{dT} &= \frac{\partial Q_{SC}}{\partial \chi_3}\frac{\partial \chi_3}{\partial T} + \frac{\partial Q_{SC}}{\partial N_d}\frac{\partial N_d}{\partial T} + \frac{\partial Q_{SC}}{\partial V_{bi}}\frac{\partial V_{bi}}{\partial T} \\ &= \sqrt{\frac{qN_D V_{bi}}{2\chi_3}}\frac{\partial \chi_3}{\partial T} + \sqrt{\frac{q\chi_3 V_{bi}}{2N_d}}\frac{\partial N_d}{\partial T} + \sqrt{\frac{q\chi_3 N_D}{2V_{bi}}}\frac{\partial V_{bi}}{\partial T} \\ &= \frac{Q_{SC}}{\sqrt{2}}\left(\frac{1}{\chi_3}\frac{\partial \chi_3}{\partial T} + \frac{1}{N_d}\frac{\partial N_d}{\partial T} + \frac{1}{V_{bi}}\frac{\partial V_{bi}}{\partial T}\right) \end{aligned} \tag{18}$$

According to Eq. 18, the pyroelectric coefficient p_i in a Schottky junction can be enhanced by using materials with a large dielectric tunability and temperature sensitive dopant density, etc. The detailed temperature dependence of the dielectric permittivity, effective dopant density and built-in potential are material specified, and remains to be resolved case by case.

When the Schottky junction absorbs heat and increases its temperature, the electric polarization generally reduces. This requires a charge redistribution from the metal interface to the semiconductor bulk through external circuit (Extended Data Fig.2c). Cooling the Schottky junction

will reverse this process and current direction. Thus, the junction outputs a displacive electric current when subjecting to a thermal perturbation.

Note that the effective dielectric permittivity χ_3 of the junction is much smaller that of pristine crystal/ceramic. The large built-in field in the depletion region depresses the dielectric permittivity due to its dielectric tunability.[29] This electric field modulated permittivity in the depletion region leads to two results. First, the temperature dependence of the effective permittivity in the junction is different from that of insulating undoped BSTO ceramic shown in Extended Data Fig. 5a. Second, the dielectric permittivity of the Au/Nb:BSTO junction is highly correlated with the other temperature-dependent parameters, such as dopant density. For example, due to the semiconductive nature, the effective dopant density of the Nb:BSTO ceramic is temperature dependent. Changing the semiconductor temperature will modulate the carrier density, which tailors the build-in field and in turn, dielectric permittivity. This contribution might actually be more important in building the effective pyroelectric coefficient than other parameters. Thus, the pyroelectric effect and its coefficient of the Au/Nb:BSTO junction has a different temperature dependence than that of bare insulating BSTO ceramic.

Schottky junction preparation: (001)-oriented Nb:$SrTiO_3$ and Nb:TiO_2 single crystals (SurfaceNet GmbH) were firstly cleaned by acetone, isopropanol and water in an ultrasonic bath. Afterwards, the crystal surface was cleaned by oxygen plasma for 60 s before sputtering gold electrodes (Cressington sputter coater 208HR). Due to this optimized preparation technique, the Schottky junctions exhibit negligible hysteresis in the current-voltage characteristics with a very low reverse bias current, i.e. highly insulating in the reverse biased conditions. This high interface quality enables high repeatability of the observed effects. The Ohmic contacts are formed by evaporating Pt (40nm)/Al (10 nm) bilayer on the crystal surface. The silicon crystals with a $0.005\ \Omega cm$ resistivity and a dopant density of 1.2×10^{25} m^{-3}. (Okmetic) were cleaned and etched by buffered oxide etcher (BOE) for 1 min to remove SiO_2 passive layer. Note that the Schottky contact and the ohmic contact were set at the same sample surface to achieve the same chemical and mechanical condition for both types of contacts during the measurements.

Nb-doped $Ba_{0.6}Sr_{0.4}TiO_3$ ceramic preparation: Undoped and 0.1% wt Nb-doped $Ba_{0.6}Sr_{0.4}TiO_3$ ceramics were prepared by the classic solid-state reaction method. Raw chemical powders TiO_2 (99.99%, Alfa Aesar), $BaCO_3$ (99.95%, Alfa Aesar), $SrCO_3$ (99.99%, Alfa Aesar), Nb_2O_3 (99.9985%, Alfa Aesar) were mixed in 2-propanol and ball milled for 4 hours. The mixed powders

were calcined at 1000 ^{o}C for 10 hours in air. The reacted powder was grounded and compressed to pellets, which were sintered in a tube furnace at 1400 ℃ for 10 hours in air. The obtained ceramic pellets (relative density of about 96%) were cut by a diamond blade saw into cuboid shape with parallel edges. To fully activate the Nb-dopant electrically, the cut pellets were annealed in the forming gas (95% N_2 + 5% H_2) at 900 ^{o}C for 6 hours. Then, the two large area ceramic surfaces were polished by diamond papers (average diamond particle diameter down to 0.5 μm). A carrier density of about 7×10^{24} m^{-3} was measured by Hall effect.

Electric properties characterization: Current-voltage and capacitance-voltage of the Schottky junctions were characterized by Keithley 2636B source meter and Keysight E4980A LCR meter, respectively. The capacitance was measured with an AC driven voltage of 100 mV at 1 kHz.

Interface direct piezoelectric effect characterization: The direct piezoelectric effect, i.e. converting mechanical energy into electrical energy, was measured by a home-built device (see Extended Data Fig. 7). The samples with two parallel sides edge were clamped between a piezoelectric actuator (P-888.51, PI Ceramic GmbH) and a micrometre head (No. 153-201, Mitutoyo Ltd). The dynamic stress that varies sinusoidally with time was generated by the piezoelectric actuator. The current generated in the Schottky junction was detected by a transimpedance amplifier (DLPCA-200, Femto) and then displayed by an oscilloscope (DSO-X 3034A, Agilent Technologies) or analysed by a Lock-in amplifier (SR865A, Stanford Research Systems).

The stress σ exerted by the piezoelectric actuator was calibrated by measuring the dynamic strain ε developed in the sample and calculated via its stiffness c, i.e. stress $\sigma_{11} = c_{11}\varepsilon_{11}$. The dynamic strain was measured by gluing a strain gauge (R=120 Ω, 632-146, RS Ltd) to the sample surface by epoxy. The resistance R of the strain gauge changes once subjected to a strain, i.e.

$$\frac{\Delta R}{R} = 2\varepsilon \qquad 19$$

The resistance variation of the strain gauge was measured with a Wheatstone bridge and a lock-in amplifier, as illustrated in Extended Data Fig. 7. The input voltage to the Wheatstone bridge was set as 1 V. The strain developed in the studied samples is in the order of magnitude of 10^{-5}, resulting in $\Delta R \ll R$. In this case, the correlation between the strain amplitude ε_0 and the lock-in output RMS value V_{RMS} equals

$$\varepsilon_0 = 2.828\, V_{RMS} \quad (20)$$

The stiffness c_{11} of Nb:$SrTiO_3$, Nb:TiO_2, and Si crystal is 318.1, 267.4 and 165.7 GPa, respectively.[30-32] The stiffness of Nb:$Ba_{0.6}Sr_{0.4}TiO_3$ ceramics is about 165 Gpa.[33]

The electromechanical coupling factor k_{31} of the Schottky junctions are calculated as:

$$k_{31} = \frac{d_{31}}{\sqrt{s_{11}\chi_s}} \quad (21)$$

where s_{11} is the elastic compliance. The s_{11} of Nb:$SrTiO_3$, Nb:TiO_2 and Nb:$Ba_{0.6}Sr_{0.4}TiO_3$ ceramics are 3.3×10^{-12} Pa^{-1}, 6.78×10^{-12} Pa^{-1}, 6.06×10^{-12} Pa^{-1}, respectively.[34,35] The effective dielectric permittivity of the Schottky junctions is calculated by linear fit according to Eq. 2. As shown by Eq. 2, the slope of the C^{-2} vs V linear fit is:

$$Slope = -\frac{2}{q\chi_3 N_d} \quad (22)$$

The doping density in these semiconductors can be estimated using their carrier density, which can be characterized by the Hall effect. The doping density of Nb:STO, Nb:TO and Nb:BSTO are measured as 2.4×10^{25} m^{-3}, 3.4×10^{25} m^{-3}, and 7×10^{24} m^{-3}, respectively. With the values of these parameters, the calculated permittivity of Au/Nb:STO, Au/Nb:TO and Au/Nb:BSTO are 1.68×10^{-9} C/Vm (ε_r=190), 1.02×10^{-9} C/Vm (ε_r= 115), 9.32×10^{-10} C/Vm (ε_r=105), respectively.

Interface converse piezoelectric effect characterization: As illustrated in Extended Data Fig. 8, the interface converse piezoelectric effect of Schottky junction was characterized by measuring the surface displacement using an atomic force microscopy system (Park XE-100). A sinusoidal-type AC voltage with a variable amplitude of V_a and frequency of 22.5 kHz was applied on the noble metal electrode of the Schottky junction via a tungsten probe. The resultant surface displacement due to the converse piezoelectric effect was probed by the AFM tip (PPP-EFM-50, Nanosensors) in contact mode under a loading force of 25 nN. The experiments were carefully designed, i.e. by applying AC bias to the gold electrode via a probe and using a conductive AFM tip that forms good electrical contact with the gold electrode, to eliminate any electrostatic contribution in the characterization. The dynamic vibration of the AFM tip is sensed by the position sensitive photodiode (PSPD) in the AFM system. The PSPD outputs a dynamic $|A-B|$ signal, magnitude of which is proportional to the surface displacement amplitude Δl. The $|A-B|$ signal is analysed by the lock-in amplifier which outputs an RMS value V_{RMS} proportional to the amplitude of $|A-B|$ signal with a ratio of 1.414. The dependence of the $|A-B|$signal on the tip displacement was

calibrated by the force-distance curve, which shows a tip sensitivity of about η=21.4 mV/nm (Extended Data Fig. 8b). Therefore, the Schottky surface vibration amplitude Δl can be estimated as:

$$\Delta l = \frac{1.414 V_{RMS}}{\eta} \quad (23)$$

Thus, the converse piezoelectric constant d_{33} of the Schottky junction is

$$d_{33} = \frac{1.414 \cdot V_{RMS}}{\eta V_a} \quad (24)$$

Interface pyroelectric effect characterization: The interface pyroelectric effect of the Schottky junctions was measured by a home-built device, as schematically shown in Extended Data Fig. 9. The sample was attached to two stages Peltier cooler, one used for controlling the global temperature and the other for inducing the alternative temperature variation using a signal generator (TTI TGA1241). The current output by the sample was amplified by a transimpedance amplifier (Femto DPLC 200) and then displayed by the oscilloscope or analysed by the lock-in amplifier. The Peltier plate and the sample were mounted in an aluminium box which can be vacuumed by a membrane pump. The temperature of the sample is varied sinusoidally with respect to time as:

$$T = T_0 + \Delta T sin(2\pi f t) \quad (25)$$

where T_0 is the base temperature, ΔT is the temperature variation amplitude and f is the frequency. The pyroelectric coefficient can be calculated as:

$$p_i = \frac{J}{2\pi f \Delta T} \quad (26)$$

Where J is the amplitude of the measured pyroelectric current density.

To characterize the light-induced pyroelectric current, the samples were mounted in vacuum and illuminated by a red laser on the top electrode with a wavelength of 660 nm and light intensity of 200 mW/cm^2. The $Pb(Zr_{0.2}Ti_{0.8})_3$ and Nb:BSTO ceramics are of equal size in dimension and volume. Based on Fig.3c and 3d, we conclude that the overall behaviour of the Schottky junctions is a rather thin film-like than bulk-like, supporting the hypothesis that the signal is generated within a skin layer (depletion width) underneath the surface.

The figure of merit (F_V) of the Schottky junctions are calculated as:[7]

$$F_V = \frac{p_i}{c_p \chi_3} \quad (27)$$

where p_i is the pyroelectric coefficient, c_p is the specific heat capacity. The specific heat capacity of Nb:STO, Nb:TO and Nb:BSTO is about 2.7 J/m^{3}K.[36] The specific heat capacity of silicon is 1.65 J/m^{3}K.

Phenomenological theory of interface piezoelectricity: The volume density of internal energy U of a body subjected to external stresses σ and electric field E can be expressed in the form:[8]

$$dU = \sigma_{ij} d\varepsilon_{ij} + E_m dP_m + TdS \tag{28}$$

where ε is the strain, P is the electric polarization, T is the temperature and S is the volume density of entropy. Einstein summation convention is used here. Here, we choose (σ, E, S) as the independent variables, with the (ε, P, T) as the dependent variables. Accordingly, we introduce the enthalpy H per unit volume, defined by:

$$H = U - \sigma_{ij}\varepsilon_{ij} - E_m P_m \tag{29}$$

Hence,

$$dH = -\varepsilon_{ij} d\sigma_{ij} - P_m dE_m + TdS \tag{30}$$

As can be seen from above equation, the dependent variables can be expressed as

$$\varepsilon_{ij} = -\frac{\partial H}{\partial \sigma_{ij}}, \quad P_m = -\frac{\partial H}{\partial E_m}, \quad T = \frac{\partial H}{\partial S} \tag{31}$$

Since the entropy is as a constant in the adiabatic conditions, the dependent variables of interest (ε, E) are function of stress σ and polarization P:

$$\varepsilon_{ij} = \varepsilon(\sigma_{kl}, E_n);\ P_m = P(\sigma_{kl}, E_n); \tag{32}$$

Expanding above functions to the second order about the position of zero strain and zero electric polarization, we can get

$$\varepsilon_{ij} = \frac{\partial \varepsilon_{ij}}{\partial \sigma_{kl}}\sigma_{kl} + \frac{\partial \varepsilon_{ij}}{\partial E_n}E_n + \frac{1}{2!}\left[\frac{\partial^2 \varepsilon_{ij}}{\partial \sigma_{kl}\partial \sigma_{qr}}\sigma_{kl}\sigma_{qr} + 2\frac{\partial^2 \varepsilon_{ij}}{\partial \sigma_{kl}\partial E_n}\sigma_{kl}E_n + \frac{\partial^2 \varepsilon_{ij}}{\partial E_n \partial E_o}E_n E_o\right] \tag{33}$$

$$P_m = \frac{\partial P_m}{\partial E_n}E_n + \frac{\partial P_m}{\partial \sigma_{kl}}\sigma_{kl} + \frac{1}{2!}\left[\frac{\partial^2 P_m}{\partial \sigma_{kl}\partial \sigma_{qr}}\sigma_{kl}\sigma_{qr} + 2\frac{\partial^2 P_m}{\partial \sigma_{kl}\partial E_n}\sigma_{kl}E_n + \frac{\partial^2 P_m}{\partial E_n \partial E_o}E_n E_o\right] \tag{34}$$

The first two differentiation terms in Eq. 33 & 34 represent the elastic compliance and the reciprocal of dielectric susceptibility, respectively.

$$\frac{\partial \varepsilon_{ij}}{\partial \sigma_{kl}} = s_{ijkl}^{P} \quad (35)$$

$$\frac{\partial P_m}{\partial E_n} = \chi_{mn}^{\sigma} \quad (36)$$

The fourth-order tensor s_{ijkl}^{P} is the elastic compliance measured at constant electric polarization and the second-order tensor χ_{mn}^{σ} denotes the dielectric permittivity measured at constant stress. The second first-order differentiation in Eq. 33 & 34 represents the converse and direct piezoelectric effect in non-centrosymmetric materials.

$$\frac{\partial \varepsilon_{ij}}{\partial E_n} = \frac{\partial P_n}{\partial \sigma_{ij}} = d_{nij} \quad (37)$$

For simplicity, we assume the piezoelectric constants remains constant under external stress. Thus,

$$\frac{\partial^2 \varepsilon_{ij}}{\partial \sigma_{kl} \partial E_n} = \frac{\partial d_{nij}}{\partial \sigma_{kl}} = 0 \quad (38)$$

$$\frac{\partial^2 P_m}{\partial \sigma_{kl} \partial \sigma_{qr}} = \frac{\partial d_{mkl}}{\partial \sigma_{qr}} = 0 \quad (39)$$

It is also reasonable to assume that the elastic constant of the crystals remains unchanged under external stress, namely, $\frac{\partial^2 \varepsilon_{ij}}{\partial \sigma_{kl} \partial \sigma_{qr}} = 0$. And the dielectric susceptibility remains constant under small external electric field, i.e. $\frac{\partial^2 P_m}{\partial E_n \partial E_o} = 0$.[6] Also, the other second-order partial derivatives are correlated:

$$\frac{\partial^2 \varepsilon_{ij}}{\partial E_n \partial E_o} = -\frac{\partial^3 H}{\partial \sigma_{ij} \partial E_n \partial E_o} = \frac{\partial^2 P_o}{\partial \sigma_{ij} \partial E_n} = 2M_{ijno} \quad (40)$$

The derived fourth-rank tensor M_{ijno} is the electrostriction coefficient in the unit of m^2/V^2. Therefore, the strain ε_{ij} and electric polarization P_m induced by external stress σ_{kl} and electric filed E_n can be written as

$$\varepsilon_{ij} = s_{ijkl}^{P} \sigma_{kl} + d_{nij} E_n + M_{ijno} E_n E_o \quad (41)$$

$$P_m = \chi_{mn}^{\sigma} E_n + d_{mkl} \sigma_{kl} + 2M_{klnm} E_n \sigma_{kl} \quad (42)$$

In the case of materials without inversion symmetry, the external applied electric field induces mechanical strain via both converse piezoelectric effect and electrostriction effect. The strain induced by the electrostriction effect in piezoelectric materials is normally much smaller than that induced by the piezoelectric effect and thus, is generally ignored. When just applying external stress to the piezoelectric materials without applying electric field, it would generate an electric polarization only by the direct piezoelectric effect.

In the case of centrosymmetric materials, piezoelectric constants d_{nij} are all zero. Eq. 41 and 42 can be rewritten as

$$\varepsilon_{ij} = s^P_{ijkl}\sigma_{kl} + M_{ijno}E_nE_o \quad (43)$$

$$P_m = \chi^\sigma_{mn}E_n + 2M_{klnm}E_n\sigma_{kl} \quad (44)$$

According to Eq. 43, the external electric field can induce mechanical strain only through the electrostriction effect. On the other hand, homogenous mechanical stress cannot induce electric polarization along in these materials due to the inversion symmetry. However, the second term in the right of Eq. 44 indicates that external stress can modulate electric polarization via electrostriction effect if there is an electric field E_n, which could be either an externally applied field or a built-in space charge field. The effective piezoelectric effect is given as

$$d_{mkl} = 2M_{klnm}E_n = 2M_{klmn}E_n \quad (45)$$

This can be understood that the electric field, that is unidirectional vector, breaks the inversion symmetry in native centrosymmetric materials, inducing electric polarization and giving rise to a piezoelectric effect via the electrostriction. We can unveil the underlying mechanism by rewriting Eq. 40 as

$$2M_{ijno} = \frac{\partial^2\varepsilon_{ij}}{\partial E_n\partial E_o} = \frac{\partial^2 P_n}{\partial E_o\partial\sigma_{ij}} = \frac{\partial\chi^\sigma_{no}}{\partial\sigma_{ij}} \quad (46)$$

Keeping in mind that:

$$\frac{\partial\varepsilon_{ij}}{\partial E_n} = \frac{\partial}{\partial E_n}\left(-\frac{\partial H}{\partial\sigma_{ij}}\right) = \frac{\partial}{\partial\sigma_{ij}}\left(-\frac{\partial H}{\partial E_n}\right) = \frac{\partial P_n}{\partial\sigma_{ij}} \quad (47)$$

According to Eq. 46, the electrostriction is a measure of the dependence of dielectric permittivity on external stress.[37] This is termed the converse electrostriction effect. Therefore, the external stress would modulate the dielectric permittivity via electrostriction effect, giving rise to a change in the electric polarization induced by electric field E_n.

Similarly, the second term in the left of the Eq. 43 also indicates the electric field E_n can also induce a converse piezoelectric effect in a centrosymmetric material. To derive the corresponding converse piezoelectric coefficient, one shall extend the Einstein notation in Eq. 43:

$$\varepsilon_{ij} = s^P_{ijkl}\sigma_{kl} + M_{ijnn}E_n^2 + 2M_{ijnq}E_nE_q \quad (48)$$

Note that the subscript $n \neq q$ in above equation. For the case of interest here, the electric field exerted on a centrosymmetric material consists of a constant part E_n, which represents the built-in field, and

an alternative component ΔE_n due to an externally applied AC voltage. Accordingly, the Eq. 48 can be rewritten as

$$\varepsilon_{ij} = s^P_{ijkl}\sigma_{kl} + M_{ijnn}{E_n}^2 + 2M_{ijnn}E_n\Delta E_n + M_{ijnn}{\Delta E_n}^2 \quad (49)$$

The first and the second term in the right of Eq. 49 represents the static strain induced by external stress and the built-in electric field in the space charged region, respectively; the third term represent the first order harmonic strain induced by the dynamic electric field, i.e. the converse piezoelectric effect; the last term is the second-harmonic strain refers to the conventional electrostriction strain. Therefore, the effect converse piezoelectric coefficient is the third term of Eq. 49:

$$d_{nij} = 2M_{ijnn}E_n \quad (50)$$

In the case that the external field E_q is in the different direction with respect to the built-in field E_n, the external field induced strain is represented by the third term in the right of Eq. 48, i.e. $\varepsilon_{ij} = 2M_{ijnq}E_nE_q$. Clearly, the corresponding piezoelectric coefficient is

$$d_{qij} = 2M_{ijnq}E_n = 2M_{ijqn}E_n \quad (51)$$

The piezoelectric coefficient expressed in Eq. 45, 50, 51 can be transformed into a unified form given as:

$$d_{mkl} = 2M_{klmn}E_n \quad (52)$$

In summary, both direct and converse piezoelectric effect with the same coefficients can occur in centrosymmetric materials once they are subjected to an electric field E_n.

References

28 Tagantsev, A.K. Piezoelectricity and flexoelectricity in crystalline dielectrics, *Phys. Rev. B* **34**, 5883-5889 (1986).

29 Tagantsev, A.K., Sherman,V.O., Astafiev, K.F., Venkatesh, J. & Setter, N. Ferroelectric Materials for Microwave Tunable Applications. *J. Electroceram.* **11**, 5-66 (2003).

30 Schranz, W., Sondergeld, P., Kityk, A. & Salje, E. K. H. Elastic properties of $SrTiO_3$ crystals at ultralow frequencies. *Phase Tran.* **69**, 61-76 (1999).

31 Grimsditch, M. & Ramdas, A. Elastic and elasto-optic constants of rutile from a Brillouin scattering study. *Phys. Rev. B* **14**, 1670 (1976).

32 Mason, W. P. Physical acoustics and the properties of solids. *J. Acoust Soc. Am.* **28**, 1197-1206 (1956).

33 Kaushal, A., Olhero, S. M., Antunes, P., Ramalho, A. & Ferreira, J. M. F. Structural, mechanical and dielectric properties of $Ba_{0.6}Sr_{0.4}TiO_3$—The benefits of a colloidal processing approach. *Mater. Res. Bull.* **50**, 329-336 (2014).

34 Pointexter, E. and Giardini, A.A. Elastic constant of strontium titanate ($SrTiO_3$), *Phys. Rev.* **110**, 1069 (1958).

35 Watchtman, J.B., Tefft, W.E. and Lam., D.G. Elastic constants of rutile (TiO_2), *J. Res. Natl, Stan. Sec. A*. **66A**, 465-471 (1962).

36 Duran, A., Morales, F., Fuentes, L. and Siqueiros, J.M., Specific heat anomalies at 37, 105 and 455 K in $SrTiO_3$:Pr, *J. Phys.: Condens. Matter*. **20**, 085219 (2008).

37 Devonshire, A.F. Theory of ferroelectrics, *Adv. Phys.* **3**, 85-130 (1954).

Data Availability: The data that support the findings of this study are available at the University of Warwick open access research repository (http://wrap.warwick.ac.uk/136971) or from the corresponding authors upon request.

Acknowledgements:

M.A. acknowledges the Theo Murphy Blue-sky Awards of Royal Society. The work was partly supported by the EPSRC (UK) through grants no. EP/M022706/1, EP/P031544/1 and EP/P025803/1. Z.M. and J.Z. acknowledge the National Natural Science Foundation of China (11772207); Natural Science Foundation of Hebei Province for Distinguished Young Scholar (A2019210204) and Shenzhen Peacock Team Program (KQTD20170810160424889). The authors acknowledge the discussion with Mr. Hangbo Zhang, Mr. Affan N. Iqbal and Dr. Fuwei Zhuge. The authors also acknowledge the technical support from Mr. Crosbie Michael.

Author Contributions:

M.M.Y and M.A conceived the idea, designed the experiments, collected the data, and wrote the manuscript. M.M.Y developed the theory. Z.D.L, Z.M. J.Z. and S.P.E were involved in sample preparation.

Competing Interests: The authors declare no competing interests.

Additional information

Correspondence and requests for materials should be addressed to M.M.Y or M.A.

Extended Data Figure Legends

Extended Data Fig. 1| Electrical field engineered symmetry in (001)-oriented Nb:$SrTiO_3$ and Nb:TiO_2 crystals a, Schematic shows the common group of $m\bar{3}m$ point group and ∞m group. **b**, Schematic shows the common group of 4/mmm point group and ∞m group. Only the rotation symmetry elements are shown here while the mirror symmetry elements are omitted. The symbol $\cap$ represents the intersect operation.

Extended Data Fig. 2| Microscopic processes of interface piezo-/pyroelectric effects. **a**, The electric polarization and compensating charges of the Schottky junction in the equilibrium state. **b**, Charge redistribution when the junction is subjected to a tensile stress. **c**, The charge redistribution when subjecting to heating. The piezo-/pyroelectric effects persist whenever there is a depletion region with a built-in field. However, another factor, i.e. the effective barrier, that assures good insulating properties in reverse bias conditions, is critical for the ability of the junction to deliver displacive current and consequently to output electricity. If the barrier becomes leaky, e.g. by a further increased temperature, the re-distribution of charge carriers will happen by electron transmission directly cross the interface via either tunnelling or thermionic emission. In this case, the pyroelectric effect might still be there, but it is screened by alternative conducting channels. This is to certain extend similar to the situation of a solar cell affected by a low shunt resistance.

Extended Data Fig. 3| Electric characterization of Al/Nb:$SrTiO_3$/Al and Au/Nb:TiO_2 junction. **a**, C^{-2}-V curve of the Au/Nb:$SrTiO_3$ junction in a large voltage range. Current-voltage curves of **b**, Al/Nb:$SrTiO_3$/Al, **c**, Au/Nb:TiO_2/Al and **d**, Al/Nb:TiO_2/Al heterostructures. **e**, C^{-2}-V curve of Au/Nb:TiO_2/Al junction. **f**, The C^{-2}-V curve of Au/Nb:TiO_2/Al junction and its linear fit near zero voltage. Given the dopant density of 3.4×10^{25} m^{-3} in Nb:TiO_2, this fit indicates the effective permittivity of the Au/ Nb:TiO_2 junction is 1.02×10^{-9} C/Vm and a built-in potential of 1.45 V. Since we mainly concern here the piezoelectric effect of the Schottky junctions without applying bias (i.e. near zero voltage), the electrical parameters derived by fitting around the zero-voltage bias give a well description of the junction properties and lead to a quantitative prediction of the piezoelectric effect consistent with experimental results.

Extended Data Fig. 4| Current output by the Nb:$SrTiO_3$ and Nb:TiO_2 crystals with Ohmic contacts and charges generated in Schottky junctions. Current density generated by **a**) the Al/Nb:$SrTiO_3$/Al heterostructure and **b**) Al/Nb:TiO_2/Al heterostructure under the stimuli of external stress. Clearly, the current density waveforms generated in the crystals with Ohmic contacts not only show a low magnitude compared to that shown in Fig. 2 of the main test but also an irregular time dependence. This demonstrates both crystals with Ohmic contacts possess no piezoelectric effect. Charge waveforms generated in Au/Nb:$SrTiO_3$/Al junction driven by dynamic **c**) stress and **d**) temperature by integrating the generated current with respect to time in Fig. 2b and Fig.3a of the main text.

Extended Data Fig. 5| Electric characterization of Au/Nb:$Ba_{0.6}Sr_{0.4}TiO_3$ junction. a, Temperature dependent dielectric constant of the insulating $Ba_{0.6}Sr_{0.4}TiO_3$ ceramic. **b**, Current density-voltage curve and **c**, Capacitance-voltage curve of the Au/Nb:$Ba_{0.6}Sr_{0.4}TiO_3$ junction.

Extended Data Fig. 6| Negligible piezoelectricity in Ohmic contacted ceramics. a, The current density output by the Au/Nb:$Ba_{0.6}Sr_{0.4}TiO_3$/Ga-In (black line) and Ga-In/Nb:$Ba_{0.6}Sr_{0.4}TiO_3$/Ga-In (red line) driven by sinusoidally varied stress (top). **b**, The current density generated by the Ga-In/$Ba_{0.6}Sr_{0.4}TiO_3$/Ga-In heterojunctions under a sinusoidally varied stress. Note that the current density amplitude observed in both ceramics with only Ohmic contacts are three to four order of magnitude smaller than that generated in the Au/Nb:$Ba_{0.6}Sr_{0.4}TiO_3$ junction, demonstrating the essential role of the Schottky contact in the induced piezoelectric effect.

Extended Data Fig. 7| Direct piezoelectric effect characterization setup.

Extended Data Fig. 8| Converse piezoelectric effect characterization. a, Schematic showing the measurement setup. **b**, Force-distance curve of PPP-EFM-50 (Nanosensors) on the Au/Nb:$SrTiO_3$.

Extended Data Fig. 9| Pyroelectric effect characterization setup.

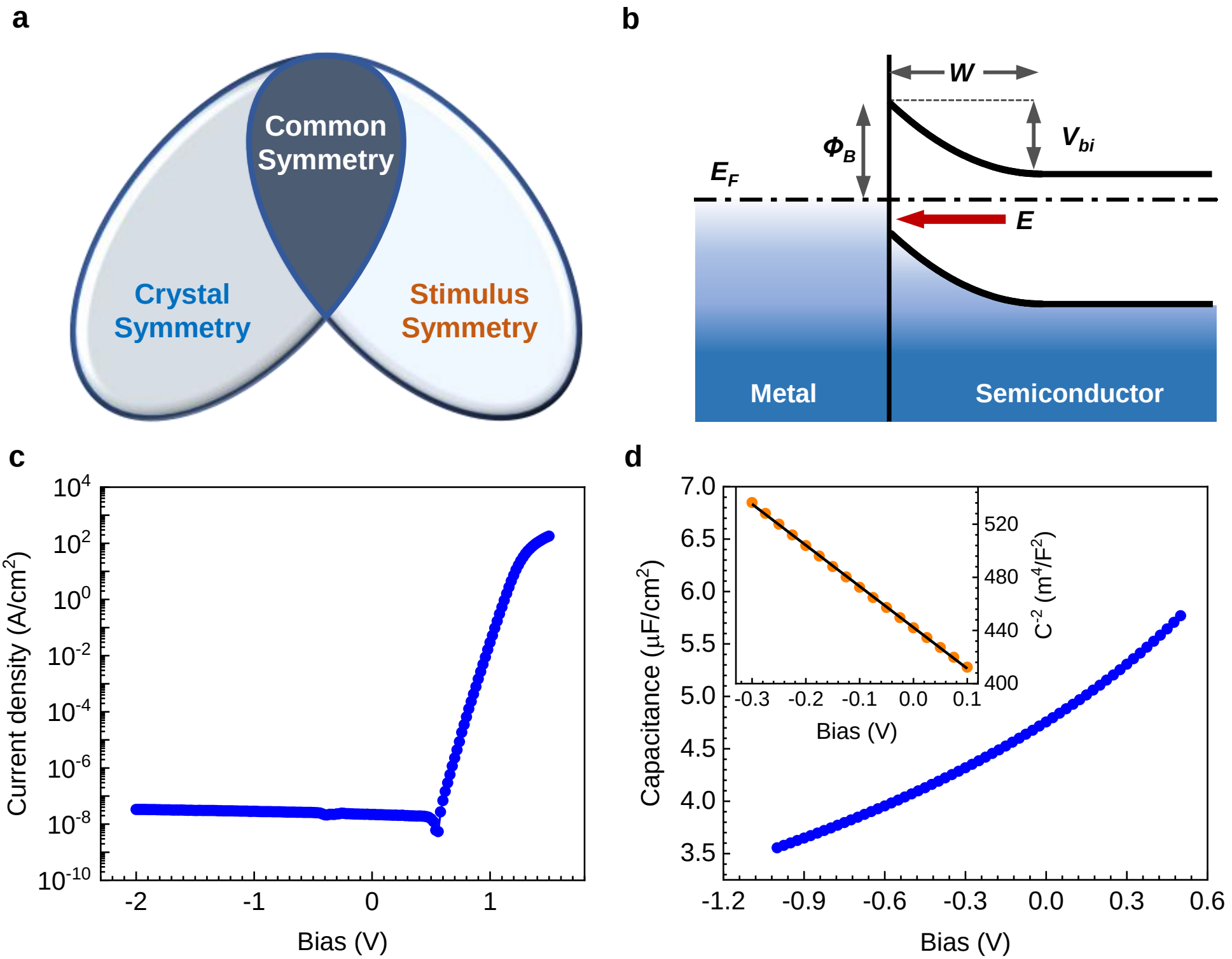
a
Common Symmetry
Crystal Symmetry
Stimulus Symmetry
b
W
Φ_B
V_{bi}
E_F
E
Metal
Semiconductor
c
Current density (A/cm^2)
10^4
10^2
10^0
10^{-2}
10^{-4}
10^{-6}
10^{-8}
10^{-10}
-2
-1
0
1
Bias (V)
d
Capacitance (μF/cm^2)
7.0
6.5
6.0
5.5
5.0
4.5
4.0
3.5
-1.2
-0.9
-0.6
-0.3
0.0
0.3
0.6
Bias (V)
520
480
440
400
C^{-2} (m^4/F^2)
-0.3
-0.2
-0.1
0.0
0.1
Bias (V)

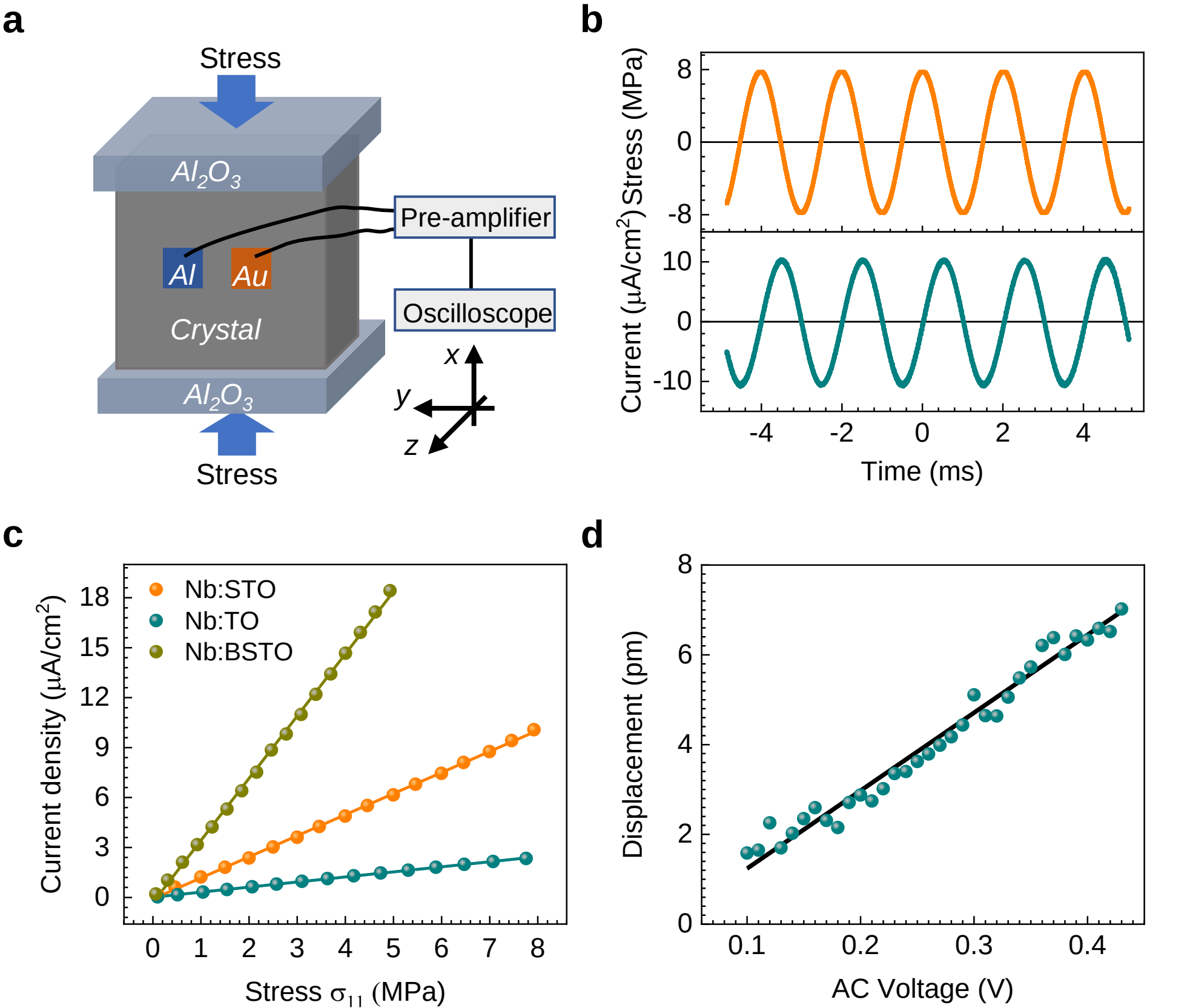
a
Stress
Al_2O_3
Al
Au
Crystal
Al_2O_3
Stress
Pre-amplifier
Oscilloscope
x
y
z
b
Current (μA/cm²)
Stress (MPa)
8
0
-8
10
0
-10
-4
-2
0
2
4
Time (ms)
c
Current density (μA/cm²)
Nb:STO
Nb:TO
Nb:BSTO
18
15
12
9
6
3
0
0
1
2
3
4
5
6
7
8
Stress σ_{11} (MPa)
d
Displacement (pm)
8
6
4
2
0
0.1
0.2
0.3
0.4
AC Voltage (V)

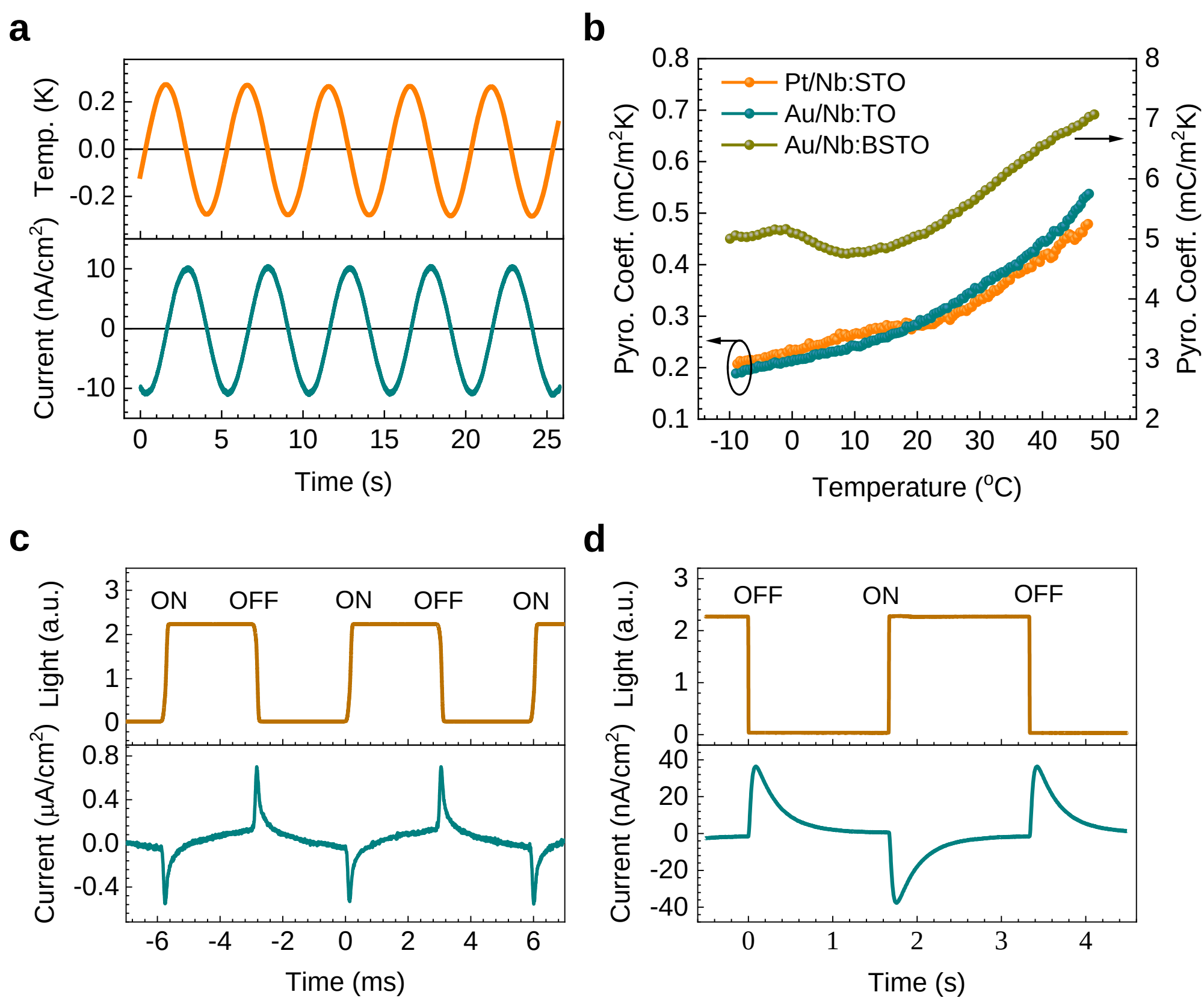
a
Temp. (K)
0.2
0.0
-0.2
Current (nA/cm^2)
10
0
-10
0
5
10
15
20
25
Time (s)
b
Pt/Nb:STO
Au/Nb:TO
Au/Nb:BSTO
Pyro. Coeff. (mC/m^{2}K)
0.8
0.7
0.6
0.5
0.4
0.3
0.2
0.1
8
7
6
5
4
3
2
-10
0
10
20
30
40
50
Temperature (^{o}C)
c
Light (a.u.)
ON
OFF
ON
OFF
ON
3
2
1
0
Current (μA/cm^2)
0.8
0.4
0.0
-0.4
-6
-4
-2
0
2
4
6
Time (ms)
d
Light (a.u.)
OFF
ON
OFF
3
2
1
0
Current (nA/cm^2)
40
20
0
-20
-40
0
1
2
3
4
Time (s)

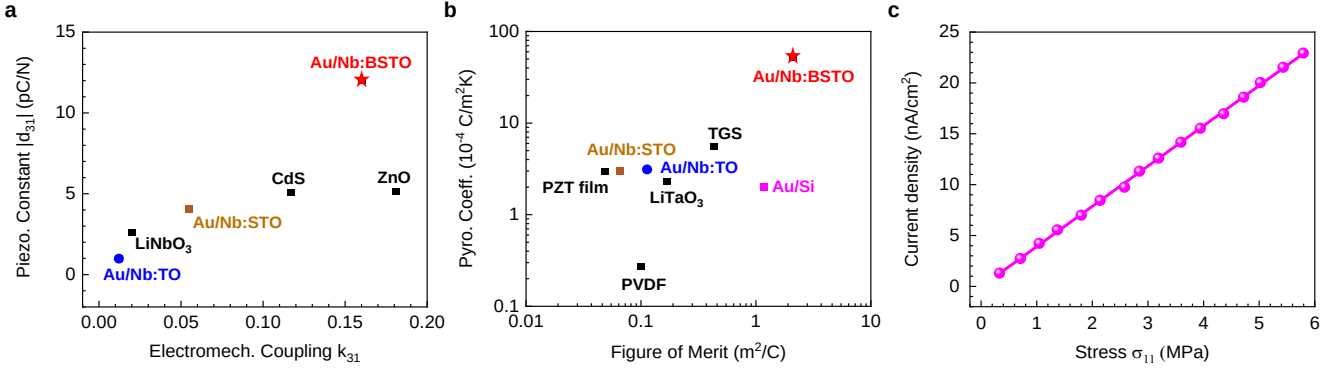
a
Piezo. Constant |d31| (pC/N)
Electromech. Coupling k31
Au/Nb:BSTO
CdS
ZnO
Au/Nb:STO
LiNbO3
Au/Nb:TO
b
Pyro. Coeff. (10-4 C/m2K)
Figure of Merit (m2/C)
Au/Nb:BSTO
TGS
Au/Nb:STO
Au/Nb:TO
PZT film
LiTaO3
Au/Si
PVDF
c
Current density (nA/cm2)
Stress σ11 (MPa)